

## Low-energy $\eta$ -nucleon interaction studied with $\eta$ photoproduction off the deuteron

S. X. Nakamura,<sup>1,2</sup> H. Kamano,<sup>3,4</sup> and T. Ishikawa<sup>5</sup>

<sup>1</sup>*Department of Physics, Osaka University, Toyonaka, Osaka 560-0043, Japan*

<sup>2</sup>*Laboratório de Física Teórica e Computacional-LFTC, Universidade Cruzeiro do Sul, São Paulo, SP 01506-000, Brazil*

<sup>3</sup>*KEK Theory Center, Institute of Particle and Nuclear Studies (IPNS), High Energy Accelerator Research Organization (KEK), Tsukuba, Ibaraki 305-0801, Japan*

<sup>4</sup>*J-PARC Branch, KEK Theory Center, IPNS, KEK, Tokai, Ibaraki 319-1106, Japan*

<sup>5</sup>*Research Center for Electron Photon Science (ELPH), Tohoku University, Sendai, Miyagi 982-0826, Japan*

(Received 29 April 2017; revised manuscript received 23 July 2017; published 26 October 2017)

We develop a reaction model for  $\eta$  photoproduction off the deuteron ( $\gamma d \rightarrow \eta pn$ ) and study the reaction at a special kinematics, where the photon beam energy is  $\sim 0.94$  GeV and the scattered proton is detected at  $\sim 0^\circ$ , for the purpose of determining the  $\eta$ -nucleon scattering length ( $a_{\eta N}$ ) and effective range ( $r_{\eta N}$ ). In this kinematics, the  $\eta$ -nucleon elastic rescattering is significantly enhanced while other background mechanisms are suppressed. We show that a ratio  $R$ , the  $\gamma d \rightarrow \eta pn$  cross section divided by the  $\gamma p \rightarrow \eta p$  cross section convoluted with the proton momentum distribution in the deuteron, has a very good resolving power of  $a_{\eta N}$  and  $r_{\eta N}$ . We conclude that the  $R$  data with 5% error, binned in 1 MeV width of the  $\eta$ -neutron invariant mass, can determine  $\text{Re}[a_{\eta N}]$  ( $\text{Re}[r_{\eta N}]$ ) at the precision of  $\sim \pm 0.1$  fm ( $\sim \pm 0.5$  fm), significantly narrowing down the previously estimated ranges of the parameters. To arrive at the conclusion, it is essential to use the  $\gamma d \rightarrow \eta pn$  reaction model equipped with elementary amplitudes that are well constrained by  $\pi N$  and  $\gamma N$  reaction data through a sophisticated coupled-channel analysis. This result strongly motivates the Research Center for Electron Photon Science (ELPH) at Tohoku University to measure  $R$ .

DOI: [10.1103/PhysRevC.96.042201](https://doi.org/10.1103/PhysRevC.96.042201)

The low-energy interaction between the  $\eta$  meson and the nucleon  $N$  is, as with the  $\pi N$  interaction, a basic feature of the meson-baryon dynamics. It is characterized by two complex parameters, the scattering length  $a_{\eta N}$  and effective range  $r_{\eta N}$ , defined through an effective-range expansion of the  $S$ -wave  $\eta N$  scattering amplitude:  $F_{\eta N}(k) = [k \cot \delta(k) - ik]^{-1}$  with  $k \cot \delta(k) = a_{\eta N}^{-1} + (1/2)r_{\eta N}k^2 + O(k^4)$ , where  $k$  is the on-shell  $\eta$  momentum in the center-of-mass (c.m.) frame and  $\delta(k)$  the phase shift. Because  $a_{\eta N}$  determines the attractive or repulsive nature of the  $\eta N$  interaction at  $k \sim 0$ , the existence of exotic  $\eta$ -mesic nuclei, which have been actively searched for experimentally, hinges on its value [1,2]. Accurate values of  $a_{\eta N}$  and  $r_{\eta N}$  can also greatly help determine the pole position of the  $S$ -wave  $N(1535)1/2^-$  resonance, the first spin-1/2 negative-parity excitation of the nucleon; the pole is known to be near the  $\eta N$  threshold but its accurate position is still uncertain [3]. It is known that the  $S$ -wave scattering parameters can well determine an  $S$ -wave resonance pole near threshold [4,5].

Despite its important role in nuclear and hadron physics, the low-energy  $\eta N$  interaction has not been well understood yet. This is attributed mainly to the fact that neither direct  $\eta N$  scattering experiments nor x-ray measurements from  $\eta$ -mesic atoms are possible due to the neutral and unstable nature of  $\eta$ , and thus one has to rely on indirect information. Previous works have attempted to extract  $a_{\eta N}$  and  $r_{\eta N}$  by analyzing the  $\pi N \rightarrow \pi N, \eta N$  and  $\gamma N \rightarrow \pi N, \eta N$  reaction data that have a sensitivity to the  $\eta N$  interaction through coupled-channel effects [2]. The  $pn \rightarrow \eta d$  reaction has also been analyzed to extract the  $\eta N$  interaction embedded in the strongly interacting  $\eta NN$  system [6]. These analyses gave fairly convergent results for the imaginary parts of  $a_{\eta N}$  and  $r_{\eta N}$ , the values of which

fall into  $\text{Im}[a_{\eta N}] = 0.2\text{--}0.3$  fm and  $\text{Im}[r_{\eta N}] = -1\text{--}0$  fm, respectively [2,7]. However, their real parts scatter in a rather wide range:  $\text{Re}[a_{\eta N}] = 0.2\text{--}0.9$  fm and  $\text{Re}[r_{\eta N}] = -6$  to  $+1$  fm. The large model dependence of the previously extracted  $\text{Re}[a_{\eta N}]$  and  $\text{Re}[r_{\eta N}]$  originates from the difficulty of isolating the  $\eta N$  scattering amplitudes from other mechanisms involved in the reactions analyzed. Therefore, it is highly desirable to utilize reactions in which mechanisms associated with the  $\eta N$  elastic rescattering are significantly enhanced while other background mechanisms being suppressed.

To meet this demand, an  $\eta$  photoproduction experiment [8] is planned at the Research Center for Electron Photon Science (ELPH), Tohoku University. In this experiment, a deuteron target is irradiated with a photon beam at the laboratory energy of  $E_\gamma \sim 0.94$  GeV [9,10], and the recoil proton from the  $\gamma d \rightarrow \eta pn$  reaction is detected at  $\theta_p \sim 0^\circ$  from the photon direction. At this chosen kinematics, an  $\eta$  is likely to be produced almost at rest, being expected to strongly interact with the spectator neutron. Meanwhile, the struck proton goes away with a large momentum, leaving little chance to interact with the  $\eta$  and neutron. This seems an ideal kinematical condition, to which we refer as the ELPH kinematics, to determine the low-energy  $\eta N$  scattering parameters. In this Rapid Communication, we show with a theoretical analysis that combined cross-section data for  $\gamma d \rightarrow \eta pn$  and  $\gamma p \rightarrow \eta p$  expected to be taken at the ELPH experiment would indeed lead to significant reduction of the uncertainty of  $a_{\eta N}$  and  $r_{\eta N}$  previously extracted, thereby providing crucial constraints on the existence of  $\eta$ -mesic nuclei and the properties of  $N(1535)1/2^-$ .

The possibility of extracting  $a_{\eta N}$  from  $\gamma d \rightarrow \eta pn$  data was first explored by Sibirtsev *et al.* [11], and a fairly large

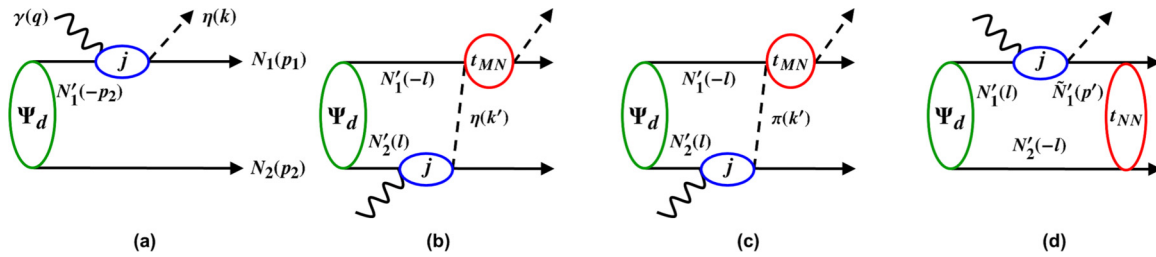


FIG. 1. Diagrammatic representation of reaction mechanisms considered in this work for  $\gamma d \rightarrow \eta N_1 N_2$ : (a) impulse, (b)  $\eta$ -exchange, (c)  $\pi$ -exchange, and (d)  $NN$ -rescattering mechanisms. Labels for particles along with their momenta in the laboratory frame are indicated. The external lines are the same for all the diagrams and thus their labels are indicated in (a) only. Also,  $\mathbf{k}' = \mathbf{q} - \mathbf{p}_2 + \mathbf{l}$  and  $\mathbf{p}' = \mathbf{q} - \mathbf{k} + \mathbf{l}$ .

$a_{\eta N}$  dependence of  $\eta$  angular and momentum distributions was shown. However, a subsequent work by Fix *et al.* [12] found a significantly less pronounced  $a_{\eta N}$  dependence than those of Ref. [11], leading to the conclusion that it is practically impossible to extract  $a_{\eta N}$  from  $\gamma d \rightarrow \eta pn$  data. Thus, until the present work, no practically useful connection has been made between  $\gamma d \rightarrow \eta pn$  data and  $a_{\eta N}$ . We note that these pioneering works [11,12] examined  $\gamma d \rightarrow \eta pn$  near the threshold ( $E_\gamma < 0.7$  GeV) while we study the reaction in rather different kinematics ( $E_\gamma \sim 0.94$  GeV;  $\theta_p \sim 0^\circ$ ).

We study  $\gamma d \rightarrow \eta pn$  relevant to the ELPH experiment with a model based on the impulse and the first-order rescattering mechanisms as depicted in Fig. 1. The  $\eta$ -exchange mechanism [Fig. 1(b)] contains the  $\eta N \rightarrow \eta N$  subprocess we are interested in, while the other mechanisms (the impulse [Fig. 1(a)],  $\pi$ -exchange [Fig. 1(c)], and  $NN$ -rescattering [Fig. 1(d)] mechanisms) are backgrounds for our purpose. With the momenta defined in Fig. 1, the amplitudes for  $T_{\text{imp}}$  (impulse),  $T_\eta$  ( $\eta$ -exchange),  $T_\pi$  ( $\pi$ -exchange), and  $T_N$  ( $NN$ -rescattering), are explicitly written in the laboratory frame as

$$T_{\text{imp}} = \sqrt{2} \sum_{s'_1} \langle \eta(\mathbf{k}) N_1(\mathbf{p}_1, s_1, t_1) | j(M_{\eta N_1}) | \gamma(\mathbf{q}, \mu) N'_1(-\mathbf{p}_2, s'_1, t_1) \rangle \langle N'_1(-\mathbf{p}_2, s'_1, t_1) N_2(\mathbf{p}_2, s_2, t_2) | \Psi_d(s_d) \rangle \quad (1)$$

$$T_{M(=\eta, \pi^\pm, \pi^0)} = \sqrt{2} \sum_{s'_1, s'_2} \sum_{t'_1, t'_2} \int d\mathbf{l} \langle \eta(\mathbf{k}) N_1(\mathbf{p}_1, s_1, t_1) | t_{MN}(M_{\eta N_1}) | M(\mathbf{q} - \mathbf{p}_2 + \mathbf{l}) N'_1(-\mathbf{l}, s'_1, t'_1) \rangle \\ \times \frac{\langle M(\mathbf{q} - \mathbf{p}_2 + \mathbf{l}) N_2(\mathbf{p}_2, s_2, t_2) | j(W) | \gamma(\mathbf{q}, \mu) N'_2(\mathbf{l}, s'_2, t'_2) \rangle}{E - E_N(\mathbf{p}_2) - E_N(-\mathbf{l}) - E_M(\mathbf{q} - \mathbf{p}_2 + \mathbf{l}) + i\epsilon} \langle N'_1(-\mathbf{l}, s'_1, t'_1) N'_2(\mathbf{l}, s'_2, t'_2) | \Psi_d(s_d) \rangle \quad (2)$$

$$T_N = \sqrt{2} \sum_{s'_1, s'_2} \int d\mathbf{l} \langle N_1(\mathbf{p}_1, s_1, t_1) N_2(\mathbf{p}_2, s_2, t_2) | t_{NN}(M_{N_1 N_2}) | \tilde{N}'_1(\mathbf{q} - \mathbf{k} + \mathbf{l}, s'_1, t_1) N'_2(-\mathbf{l}, s'_2, t_2) \rangle \\ \times \frac{\langle \eta(\mathbf{k}) \tilde{N}'_1(\mathbf{q} - \mathbf{k} + \mathbf{l}, s'_1, t_1) | j(W) | \gamma(\mathbf{q}, \mu) N'_1(\mathbf{l}, s'_1, t_1) \rangle}{E - E_N(\mathbf{q} - \mathbf{k} + \mathbf{l}) - E_N(-\mathbf{l}) - E_\eta(\mathbf{k}) + i\epsilon} \langle N'_1(\mathbf{l}, s'_1, t_1) N'_2(-\mathbf{l}, s'_2, t_2) | \Psi_d(s_d) \rangle \quad (3)$$

plus the exchange terms obtained from Eqs. (1)–(3) by flipping the overall sign and interchanging all subscripts 1 and 2 such as  $\{N_1^{(i)}, \mathbf{p}_1, s_1^{(i)}, t_1^{(i)}\} \leftrightarrow \{N_2^{(i)}, \mathbf{p}_2, s_2^{(i)}, t_2^{(i)}\}$ . The elementary (off-shell) amplitudes for photoproduction, meson-baryon, and  $NN$  rescattering are denoted by  $\langle MN | j | \gamma N' \rangle$ ,  $\langle MN | t_{MN} | M' N' \rangle$ , and  $\langle N_1 N_2 | t_{NN} | N'_1 N'_2 \rangle$ , respectively. Here,  $|\Psi_d(s_d)\rangle$  is the deuteron state at rest with spin projection  $s_d$ ;  $|N(\mathbf{p}, s, t)\rangle$  the nucleon state with momentum  $\mathbf{p}$  and spin and isospin projections  $s$  and  $t$ ;  $|\gamma(\mathbf{q}, \mu)\rangle$  the photon state with momentum  $\mathbf{q}$  and polarization  $\mu$ ; and  $|M(\mathbf{k})\rangle$  ( $M = \eta, \pi^\pm, \pi^0$ ) the pseudoscalar meson state with momentum  $\mathbf{k}$ . The total scattering energy  $E$  of the system in the laboratory frame is given by the sum of the photon laboratory energy and the deuteron rest mass,  $E = E_\gamma + m_d$ , and the invariant masses of the two-body subprocesses in the above equations are defined to be  $M_{\eta N_1} = \{[E_\eta(\mathbf{k}) + E_N(\mathbf{p}_1)]^2 - (\mathbf{k} + \mathbf{p}_1)^2\}^{1/2}$ ,

$W = \{[E - E_N(-\mathbf{l})]^2 - (\mathbf{l} + \mathbf{q})^2\}^{1/2}$ , and  $M_{N_1 N_2} = \{[E_N(\mathbf{p}_1) + E_N(\mathbf{p}_2)]^2 - (\mathbf{p}_1 + \mathbf{p}_2)^2\}^{1/2}$ , where  $E_x(\mathbf{p}) = \sqrt{m_x^2 + \mathbf{p}^2}$  with  $m_x$  being the mass of particle  $x$ .

The above definition on  $W$  would call for an explanation, because other choices of  $W$  have also been seen in the literature [13]. We calculate the mechanisms [Fig. 1(a)–1(d)] in a manner consistent with the well-established Faddeev framework up to the truncated higher order terms. The Faddeev framework uniquely specifies the energy (and thus  $W$ ) of an interacting two-body subsystem in an intermediate state. A requirement is to combine the equation with elementary (off-shell) amplitudes calculated consistently with the Faddeev framework. Our elementary amplitudes are, as discussed shortly, calculated with meson-nucleon and nucleon-nucleon potentials that perfectly fit the Faddeev framework. Meanwhile, another prescription of  $W$  corresponds to another three-dimensional scattering

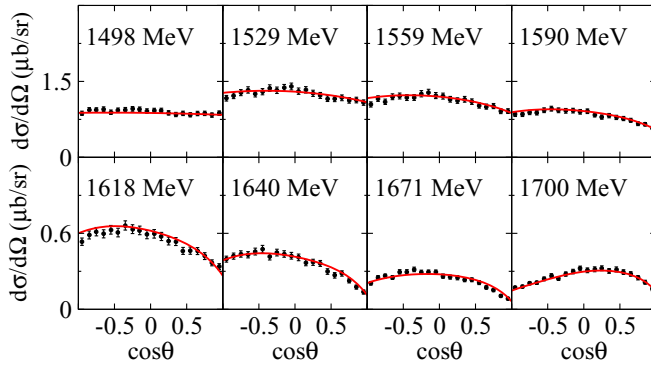


FIG. 2. Differential cross sections for  $\gamma p \rightarrow \eta p$  from the DCC model [15] in comparison with data [17] at selected invariant masses of the  $\gamma p$  system. The corresponding values of the invariant mass are indicated in each panel.

equation that should work with its own consistent elementary amplitudes but not with ours. Therefore, it does not make sense for us to use the other choices of  $W$ . However, if one uses dynamical inputs that are not consistent with any of the scattering frameworks, as has been the case in most of the past works, there is no principle to determine  $W$ , and thus various choices need to be considered.

We now specify our  $\gamma d \rightarrow \eta p n$  reaction model to evaluate Eqs. (1)–(3). The model must be built with reliable amplitudes for elementary  $\gamma N \rightarrow M N$ ,  $M N \rightarrow M' N$ , and  $N N \rightarrow N N$  processes with  $M^{(\prime)} = \pi, \eta$ , as well as with a realistic deuteron wave function, so that we can reliably isolate the amplitude for the  $\eta N \rightarrow \eta N$  subprocess from data with well-predicted contributions from all the other background mechanisms. Regarding  $\gamma N \rightarrow M N$  and  $M N \rightarrow M' N$  amplitudes, we employ those generated with a dynamical coupled-channels (DCC) model [14,15]. The DCC model is a multichannel unitary model for the  $\pi N$  and  $\gamma N$  reactions in the nucleon resonance region. It was constructed fitting  $\sim 27000$  data points, and successfully describes [14–16]  $\pi N \rightarrow \pi N, \pi \pi N, \eta N, K \Lambda, K \Sigma$  and  $\gamma N \rightarrow \pi N, \pi \pi N, \eta N, K \Lambda, K \Sigma$  reactions over the energy region from the thresholds up to  $\sqrt{s} \lesssim 2.1$  GeV. As an example, we present the  $\gamma p \rightarrow \eta p$  differential cross sections calculated with the DCC model of Ref. [15] in Fig. 2. The figure shows a very good agreement between the model and data [17] over the energy region relevant to the following calculations of  $\gamma d \rightarrow \eta p n$ . This verifies that the most important  $\gamma p \rightarrow \eta p$  amplitudes out of the elementary amplitudes for describing  $\gamma d \rightarrow \eta p n$  are well constrained by the data. This DCC model predicts the  $\eta N$  scattering parameters to be  $a_{\eta N} = 0.75 + 0.26i$  fm and  $r_{\eta N} = -1.6 - 0.6i$  fm, which are consistent with the previously estimated ranges. As for the deuteron wave function and the  $N N$  scattering amplitudes, we employ those generated with the CD-Bonn potential [18].

Previous models [11,12,19,20] also took account of the mechanisms shown in Fig. 1; the  $\pi$ -exchange mechanism was considered only in Ref. [20]. However, comparing the elementary amplitudes implemented in the previous models, the DCC model possesses unique and sound features such as

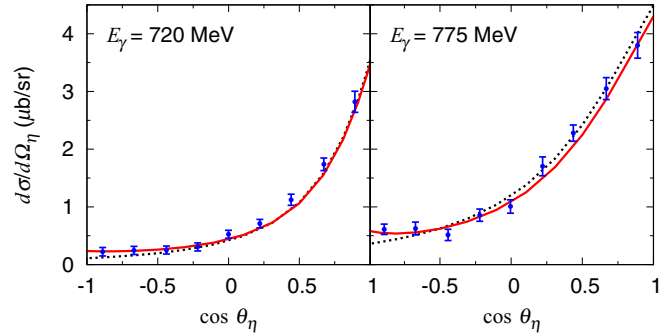


FIG. 3. Angular distributions of  $\eta$  in  $\gamma d \rightarrow \eta p n$  in the  $\gamma d$  c.m. frame. The photon laboratory energy  $E_\gamma$  is indicated in each panel. The solid curves are from the full calculation, while the dotted curves are obtained with the impulse mechanism only. The data are for the semi-inclusive  $\gamma d \rightarrow \eta X$  process [21]; the coherent contribution is negligible here [22].

(i) the model describes *all* the meson-baryon and photoproduction amplitudes relevant to  $\gamma d \rightarrow \eta p n$  in a unified manner; (ii) the model generates, by construction, off-shell amplitudes that are well suited for working with the Faddeev framework. We also note that a simple  $\gamma p \rightarrow \eta p$  model including only the  $S_{11}(1535)$ -excitation mechanism [11,19] is not enough for practically describing  $\gamma d \rightarrow \eta p n$  at the ELPH kinematics because the  $\gamma p \rightarrow \eta p$  amplitudes of  $\sqrt{s} = 1.6$ – $1.7$  GeV give a large contribution.

The setup described above allows us to make a parameter-free prediction for the  $\gamma d \rightarrow \eta p n$  cross sections. We thus confront our model predictions with existing data, thereby assessing the validity of the model. In Fig. 3, we show the  $\eta$  angular distribution at  $E_\gamma = 720$  and  $775$  MeV from our DCC-based model with and without the rescattering contributions along with the data. Our parameter-free prediction is found to be in excellent agreement with the data. A slight enhancement in the backward direction due to the  $\eta N \rightarrow \eta N$  rescattering is important for this agreement. Fix *et al.* [20] have done a comparable calculation, and found a rather minor role of the  $\eta N \rightarrow \eta N$  rescattering mechanism in the  $\eta$  angular distribution at these energies. The slight underestimation of their results at backward angles (Fig. 5 of Ref. [20]) is likely to be ascribable to the different  $\eta N$  scattering lengths:  $a_{\eta N} = 0.75 + 0.26i$  fm in our model and  $a_{\eta N} = 0.5 + 0.32i$  fm in Ref. [20]. Regarding the cross sections with the impulse mechanism only, our result is close to that of Ref. [20] while significantly smaller than that of Ref. [11]. See Ref. [12] for a detailed discussion on the difference with Ref. [11].

Now let us consider the  $\gamma d \rightarrow \eta p n$  reaction at the ELPH kinematics with  $E_\gamma = 0.94$  GeV and  $\theta_p = 0^\circ$ . In Fig. 4 (top), our model predictions for the threefold differential cross section  $d^3\sigma/dM_{\eta n}d\Omega_p$ , are presented as a function of  $M_{\eta n}$ . We find that the dominant contribution is from the impulse mechanism [Fig. 1(a)] that contains the  $\gamma p \rightarrow \eta p$  amplitudes, while the  $\gamma n \rightarrow \eta n$  amplitudes negligibly contribute. The  $\eta$ -exchange mechanism [Fig. 1(b)] has a substantial contribution to the cross section, which changes the impulse result by  $-40$  to  $+20\%$  [difference between the dashed and dotted curves in Fig. 4 (bottom)]. Meanwhile, the  $\pi$ -exchange [Fig. 1(c)]

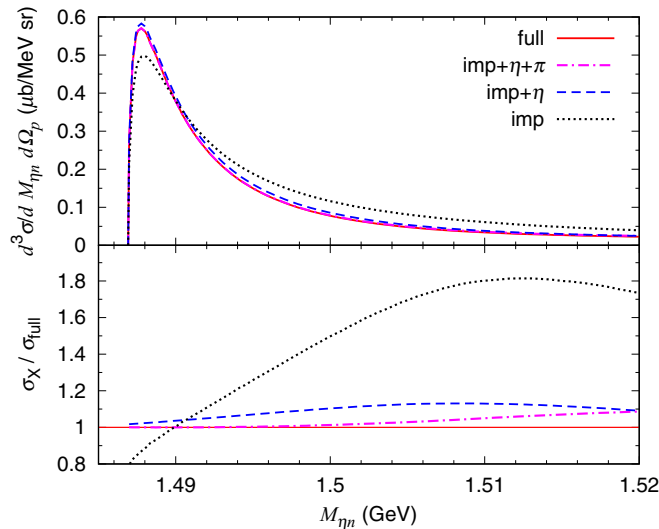


FIG. 4. (Top) Threefold differential cross section,  $d^3\sigma/dM_{\eta n}d\Omega_p$ , for  $\gamma d \rightarrow \eta pn$  at  $E_\gamma = 0.94$  GeV and  $\theta_p = 0^\circ$ , plotted as a function of  $M_{\eta n}$ . The results are from the full calculation (solid curve), the impulse mechanism only (dotted curve), the impulse and  $\eta$ -exchange mechanisms (dashed curve), and the impulse,  $\eta$ - and  $\pi$ -exchange mechanisms (dash-dotted curve). The dash-dotted curve falls almost exactly on the solid curve. (Bottom) Ratios of the differential cross sections calculated with the various mechanisms to those from the full calculation.

contribution is smaller, and suppresses the cross sections by  $\lesssim 9\%$  (difference between the dashed and dash-dotted curves). The  $NN$  rescattering [Fig. 1(d)] contribution (deviation of the dash-dotted curve from 1) is very small for  $M_{\eta n} \lesssim 1.5$  GeV. This feature is what we expect to find in this special kinematics. The  $\pi$ -exchange mechanism is strongly suppressed even though the elementary  $\gamma p \rightarrow \pi N$  amplitude is significantly larger than that of  $\gamma p \rightarrow \eta p$  at the considered energies. This is because the exchanged pions have rather large momenta near their on-shell, picking up high-momentum components with very small probabilities in the deuteron wave function. The  $NN$ -rescattering mechanism is hindered by the same kinematical reason, and also by the rather weak  $NN$  scattering at this kinematics where the  $NN$  relative momentum is large.

We have shown that the  $\gamma d \rightarrow \eta pn$  in the ELPH kinematics for  $M_{\eta n} \lesssim 1.5$  GeV are described with the impulse and  $\eta$ -exchange mechanisms and with the smaller (almost negligible) correction from the  $\pi$ -exchange ( $NN$ -rescattering) mechanism. This indicates that the proton is well separated from interacting with the  $\eta n$  system, and thus multiple rescatterings beyond the first-order rescattering [Figs. 1(b)–1(d)] should be safely neglected in this kinematical region. We have also confirmed that an off-shell momentum effect associated with the  $\eta n \rightarrow \eta n$  scattering amplitude is very small and that  $\eta n \rightarrow \eta n$  partial-wave amplitudes higher than the  $S$  wave give negligibly small contributions. These facts allow us to modify the full  $\gamma d \rightarrow \eta pn$  model by replacing the  $\eta n$  scattering amplitude with the  $S$ -wave one parametrized with  $a_{\eta N}$  and  $r_{\eta N}$ , and then to determine these parameters through analyzing the forthcoming ELPH data. To make contact with the ELPH

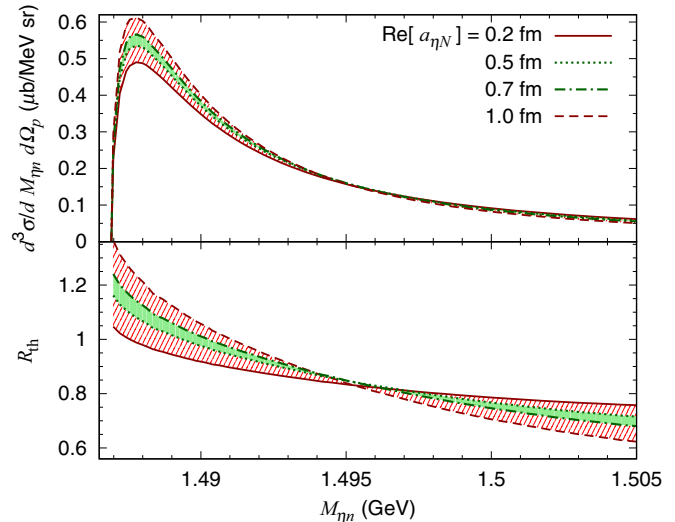


FIG. 5. (Top)  $\text{Re}[a_{\eta N}]$  dependence of  $\gamma d \rightarrow \eta pn$  differential cross sections at  $E_\gamma = 0.94$  GeV and  $\theta_p = 0^\circ$  calculated with the full model. The curves are obtained with  $\text{Re}[a_{\eta N}] = 0.2, 0.5, 0.7,$  and  $1.0$  fm;  $\text{Im}[a_{\eta N}] = 0.25$  fm, and  $r_{\eta n} = 0$ . (Bottom)  $R_{\text{th}}$  defined in Eq. (4) for various values of  $\text{Re}[a_{\eta N}]$ .

data, we need to take one more step because the data are actually given in a form of the ratio, denoted by  $R_{\text{expt}}$ , of the measured cross sections for  $\gamma d \rightarrow \eta pn$  divided by those for  $\gamma p \rightarrow \eta p$  convoluted with the proton momentum distribution in the deuteron. This is for removing systematic uncertainties of the acceptance from the detector coverage. Thus, from the theoretical side, the corresponding quantity to calculate is

$$R_{\text{th}}(M_{\eta n}) = \frac{d^3\sigma_{\text{full}}/dM_{\eta n}d\Omega_p|_{\theta_p=0^\circ}}{d^3\sigma_{\text{imp}}/dM_{\eta n}d\Omega_p|_{\theta_p=0^\circ}}, \quad (4)$$

where  $\sigma_{\text{full}}$  ( $\sigma_{\text{imp}}$ ) is calculated with the modified full model (the impulse term only). The remaining questions to address are how sensitively  $R_{\text{th}}$  changes as  $a_{\eta N}$  and  $r_{\eta N}$  are varied, and how well  $R_{\text{expt}}$  with a certain error can determine  $a_{\eta N}$  and  $r_{\eta N}$ .

First we vary  $\text{Re}[a_{\eta N}]$  over 0.2–1.0 fm, with fixed values of  $\text{Im}[a_{\eta N}] = 0.25$  fm and  $r_{\eta N} = 0$  fm. At the ELPH kinematics and  $M_{\eta n} \leq 1.505$  GeV, the obtained cross sections are mostly within the red striped region shown in Fig. 5 (top). The corresponding variation of  $R_{\text{th}}$  is shown in Fig. 5 (bottom) where the sensitivity to the variation of  $\text{Re}[a_{\eta N}]$  is more clearly seen. As the striped bands show, the cross section and thus  $R_{\text{th}}$  changes by  $\sim 25\%$  at the quasi-free (QF) peak position at  $M_{\eta n} \sim 1.488$  GeV. Meanwhile, the green solid bands, which are covered when  $\text{Re}[a_{\eta N}]$  is varied by  $\pm 0.1$  fm from 0.6 fm, have the widths of  $\sim 5\%$  at the QF peak. The result indicates that  $R_{\text{expt}}$  data of 5% error per MeV bin, which is achievable in the planned ELPH experiment [8], can determine  $\text{Re}[a_{\eta N}]$  at the precision of  $\sim \pm 0.1$  fm, significantly narrowing down the current uncertainty.

Next we vary  $\text{Re}[r_{\eta N}]$  over a rather broad range of the current estimates,  $-6$ – $0$  fm; the scattering length is fixed at  $a_{\eta n} = 0.75 + 0.26i$  fm, the value from the latest DCC analysis [15];  $\text{Im}[r_{\eta N}] = 0$  fm. The corresponding changes of the cross section and  $R_{\text{th}}$  cover the red striped region in Fig. 6. Because

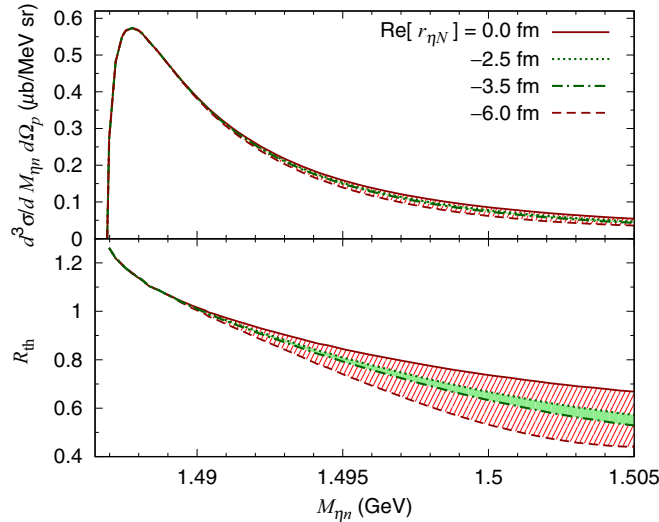


FIG. 6. Similar presentation to Fig. 5, but using  $\text{Re}[r_{\eta N}] = 0, -2.5, -3.5,$  and  $-6$  fm;  $a_{\eta n} = 0.75 + 0.26i$  fm and  $\text{Im}[r_{\eta N}] = 0$  fm are fixed.

$r_{\eta N}$  plays no role very close to the  $\eta N$  threshold, its effect starts to be visible at  $\sim 5$  MeV above the threshold. The red striped (green solid) band of  $R_{\text{th}}$  shows that  $R_{\text{th}}$  at  $M_{\eta n} = 1.5$  GeV changes by  $\sim 30\%$  ( $\sim 5\%$ ) when  $\text{Re}[r_{\eta N}]$  is varied over  $-6$ – $0$  fm ( $-3.5$  to  $-2.5$  fm). Therefore,  $R_{\text{expt}}$  data of 5% error per MeV bin can also determine  $\text{Re}[r_{\eta N}]$  at the precision of  $\lesssim \pm 0.5$  fm, significantly improved precision over the current estimates.

Regarding the imaginary part, we vary  $\text{Im}[a_{\eta N}]$  in the range of 0.2–0.3 fm, the currently estimated range, and with  $\text{Re}[a_{\eta N}] = 0.6$  fm and  $r_{\eta N} = 0$  fm. The cross sections and  $R_{\text{th}}$  change at most 5%. When varying  $\text{Im}[r_{\eta N}]$  over the currently estimated range,  $-1$ – $0$  fm, with  $a_{\eta n} = 0.75 + 0.26i$  fm and  $\text{Re}[r_{\eta N}] = 0$  fm being fixed, we found a similar situation.

We argue that theoretical uncertainties hardly affect the above results. A major part of the uncertainty of the  $\gamma d \rightarrow \eta pn$  cross section is from the elementary  $\gamma p \rightarrow \eta p$  amplitudes that take over errors ( $\sim \pm 5\%$ ) from  $\gamma p \rightarrow \eta p$  data fitted. However, what we need in analyzing the ELPH data is not the cross section itself but  $R_{\text{th}}$  in which theoretical uncertainty in the cross section is largely canceled out. We have confirmed that  $R_{\text{th}}$  is very stable ( $\lesssim 0.1\%$ ) even when the overall magnitude of the  $\gamma p \rightarrow \eta p$  amplitudes is varied over  $\pm 3\%$ . Another possible source of the uncertainty is the subthreshold  $\gamma p \rightarrow \eta p$  amplitudes which are not well constrained by the data. However, at the ELPH kinematics, the cross sections (and thus  $R_{\text{th}}$ ) are found to hardly change ( $\lesssim 0.1\%$  at the QF peak;  $\lesssim 1\%$  for  $M_{\eta n} \leq 1.505$  GeV) even when the subthreshold contributions are omitted. We have also studied the model

dependence of the deuteron wave function. We used those of the CD-Bonn [18], Nijmegen I [23], and Reid93 [23] models, and found a rather good stability ( $< 0.5\%$  at the QF peak;  $\lesssim 1\%$  at  $M_{\eta n} \sim 1.5$  GeV) of  $R_{\text{th}}$ .

Finally, we make clear what we have advanced from the previous investigations [11,12] on extracting  $a_{\eta N}$  from  $\gamma d \rightarrow \eta pn$  data. For this purpose, it would be illustrative to compare our main result (Fig. 5) with Fig. 6 (bottom) of Ref. [12] that also shows the  $a_{\eta N}$  dependence of  $\gamma d \rightarrow \eta pn$  differential cross sections at a fixed proton angle. Despite the similarity, the authors of Ref. [12] were concerned with the cross-section shape while we utilize the absolute values of  $R_{\text{th}}$  that has a significantly better sensitivity to the  $\eta N$  scattering parameters. What enables us to utilize the  $R_{\text{th}}$  values is our very well-controlled calculation as follows. At the kinematics chosen in Ref. [12] ( $E_\gamma = 670$  MeV,  $\theta_p = 18^\circ$ ,  $M_{\eta n} \sim m_\eta + m_n$ ), according to our model, we found (i) the elementary  $\gamma n \rightarrow \eta n$  amplitudes give a contribution comparable to that from the  $\gamma p \rightarrow \eta p$  amplitudes; (ii) the subthreshold  $\gamma p \rightarrow \eta p$  amplitudes give a  $\sim 30\%$  contribution; (iii) the  $NN$ -rescattering contribution is not well suppressed ( $\sim 10\%$  contribution) and thus, considering the precision in question, a contribution from multiple rescatterings beyond the first-order rescattering would be non-negligible. On the other hand, our result obtained at the ELPH kinematics is essentially free from contributions (i)–(iii) that are currently difficult to control with a high precision. Another benefit of utilizing the ELPH kinematics is that the cross sections are fairly large near the QF peak, making a precise measurement possible. Indeed, our cross sections at the QF peak in Fig. 5 are  $\sim 20$  times larger than those shown in Fig. 6 (bottom) of Ref. [12]. One more advancement is that we proposed to use the ratio, Eq. (4), to cancel out the  $\sim 5\%$  uncertainty inherent in any elementary  $\gamma p \rightarrow \eta p$  amplitudes. The advancements described above lead us to a conclusion that it will be possible to significantly improve the precision of the  $\eta N$  scattering parameters using the ELPH data.

In conclusion, we have analyzed the  $\gamma d \rightarrow \eta pn$  reaction at  $E_\gamma = 0.94$  GeV and  $\theta_p = 0^\circ$ , and found that, once  $R_{\text{expt}}$  data of 5% error binned in 1 MeV width are given,  $\text{Re}[a_{\eta N}]$  ( $\text{Re}[r_{\eta N}]$ ) can be determined at the precision of  $\sim \pm 0.1$  fm ( $\sim \pm 0.5$  fm), which is significantly better than the currently estimated uncertainty. We emphasize that for reliably extracting the  $\eta N$  scattering parameters from the data, it is prerequisite to control all the relevant subprocess in  $\gamma d \rightarrow \eta pn$  with a sophisticated model like the DCC model [14,15].

We thank T. Sato for a useful discussion. This work was supported in part by JSPS KAKENHI Grants No. JP25105010, No. JP25800149, and No. JP26400287, and Fundação de Amparo à Pesquisa do Estado de São Paulo-FAPESP, Process No. 2016/15618-8.

[1] Q. Haider and L. C. Liu, *Phys. Lett. B* **172**, 257 (1986).

[2] Q. Haider and L. C. Liu, *Int. J. Mod. Phys. E* **24**, 1530009 (2015).

[3] C. Patrignani *et al.* (Particle Data Group), *Chin. Phys. C* **40**, 100001 (2016).

[4] Y. Ikeda, T. Hyodo, D. Jido, H. Kamano, T. Sato, and K. Yazaki, *Prog. Theor. Phys.* **125**, 1205 (2011).

- [5] H. Kamano, S. X. Nakamura, T.-S. H. Lee, and T. Sato, *Phys. Rev. C* **92**, 025205 (2015).
- [6] V. Yu. Grishina, L. A. Kondratyuk, M. Buescher, C. Hanhart, J. Haidenbauer, and J. Speth, *Phys. Lett. B* **475**, 9 (2000); S. Wycech and A. M. Green, *AIP Conf. Proc.* **603**, 547 (2001); H. Garcilazo and M. T. Peña, *Eur. Phys. J. A* **38**, 209 (2008).
- [7] A. M. Green and S. Wycech, *Phys. Rev. C* **71**, 014001 (2005); **72**, 029902(E) (2005).
- [8] T. Ishikawa *et al.*, ELPH-2844 experiment, 2016 (unpublished); *JPS Conf. Proc.* **13**, 020031 (2017); *Nucl. Instrum. Methods A* **832**, 108 (2016).
- [9] T. Ishikawa *et al.*, *Nucl. Instrum. Methods Phys. Res., Sect. A* **622**, 1 (2010).
- [10] T. Ishikawa *et al.*, *Nucl. Instrum. Methods Phys. Res., Sect. A* **811**, 124 (2016).
- [11] A. Sibirtsev, S. Schneider, C. Elster, J. Haidenbauer, S. Krewald, and J. Speth, *Phys. Rev. C* **65**, 044007 (2002); **65**, 067002 (2002).
- [12] A. Fix and H. Arenhövel, *Eur. Phys. J. A* **19**, 275 (2004).
- [13] E. Breitmoser and H. Arenhövel, *Nucl. Phys. A* **612**, 321 (1997).
- [14] H. Kamano, S. X. Nakamura, T.-S. H. Lee, and T. Sato, *Phys. Rev. C* **88**, 035209 (2013).
- [15] H. Kamano, S. X. Nakamura, T.-S. H. Lee, and T. Sato, *Phys. Rev. C* **94**, 015201 (2016).
- [16] H. Kamano, *Phys. Rev. C* **88**, 045203 (2013).
- [17] O. Bartholomy *et al.*, *Eur. Phys. J. A* **33**, 133 (2007); V. Crede *et al.*, *Phys. Rev. C* **80**, 055202 (2009); E. F. McNicoll *et al.*, *ibid.* **82**, 035208 (2010).
- [18] R. Machleidt, *Phys. Rev. C* **63**, 024001 (2001).
- [19] A. Fix and H. Arenhövel, *Z. Phys. A* **359**, 427 (1997).
- [20] A. Fix, H. Arenhövel, M. Levchuk, and M. Tammam, *Phys. Rev. C* **91**, 014001 (2015).
- [21] B. Krusche *et al.*, *Phys. Lett. B* **358**, 40 (1995).
- [22] J. Weiß *et al.*, *Eur. Phys. J. A* **11**, 371 (2001).
- [23] V. G. J. Stoks, R. A. M. Klomp, C. P. F. Terheggen, and J. J. de Swart, *Phys. Rev. C* **49**, 2950 (1994).